PHYSICAL REVIEW E **78**, 045603(R) (2008)

Local nanofluidic light sources in silicon photonic crystal microcavities

Silvia Vignolini,[1,*] Francesco Riboli,[1] Francesca Intonti,[2,1] Michele Belotti,[3,4] Massimo Gurioli,[1] Yong Chen,[4,5] Marcello Colocci,[1] Lucio Claudio Andreani,[3] and Diederik S. Wiersma[1]

[1]*European Laboratory for Non-linear Spectroscopy (LENS) and INFM-BEC, Via N. Carrara, 1, I-50019 Sesto Fiorentino Firenze, Italy*

[2]*CNISM, Unità di Ricerca di Firenze, 50019 Sesto Fiorentino, Italy*

[3]*Dipartimento di Fisica "A. Volta" and UdR CNISM, Università degli Studi di Pavia, Via Bassi 6, I-27100 Pavia, Italy*

[4]*Laboratoire de Photonique et de Nanostructures, LPN-CNRS, Route de Nozay, F-91460 Marcoussis, France*

[5]*Département de Chimie, Ecole Normale Supérieure, 24 Rue Lhomond, F-75231 Paris Cedex 05, France*

(Received 28 July 2008; published 30 October 2008)

We report on the realization of a rewritable and local source inside a Si-based photonic crystal microcavity by infiltrating a solution of colloidal PbS quantum dots inside a single pore of the structure. We show that the resulting spontaneous emission from the source is both spatially and spectrally redistributed due to the mode structure of the photonic crystal cavity. The coupling of the quantum dot emission to the cavity mode is analyzed by mapping the luminescence signal of the infiltrated solution with a scanning near-field optical microscope at room temperature. Spectral characterization and the mode profile are in good agreement with a three-dimensional numerical calculation of the system.

DOI: 10.1103/PhysRevE.78.045603 PACS number(s): 42.70.Qs, 47.61.−k, 68.37.Uv, 78.67.Hc

By local structuring a photonic crystal it is possible to realize microresonators, waveguides, and possible several other photonic components. The opportunity to insert a light-emitting element in such structures is of interest both for their potential applications and for their fundamental physical properties [1–5]. A versatile approach to achieve this is via the use of colloidal quantum dots. In first experiments such quantum dot solutions were globally infiltrated in the entire photonic crystal by simply immersing the sample in a quantum dot suspension [6–9]. While these initial studies show that it is possible to achieve weak coupling between colloidal quantum dot sources and the modes of the photonic crystal, this technique does not allow one to create local sources that can be combined with other functionalities in photonic crystals.

In this paper we report on the realization of an active structure based on *local* infiltration of liquids in a photonic crystal. In particular, we realize a rewritable local source in the telecom window (at 1.3 μm) inside a silicon photonic crystal microcavity. By using a commercial scanning near-field optical microscope (SNOM) we are able to map and reconstruct the emission spectrum of the infiltrated source with a spatial resolution of $\lambda/5$. The opportunity of having simultaneously information about the topography of the sample and the optical signal from the local source permits us to localize the signal in well-defined positions around the cavity and to access the spatial distribution of the optical modes. We clearly observe the effect of mode coupling between source and photonic crystal cavity and a corresponding spectral redistribution of the emission intensity.

The investigated sample is a two-dimensional (2D) photonic crystal cavity realized in a suspended silicon membrane with a thickness $w=260$ nm. A triangular lattice of air holes with lattice constant $a=350$ nm and hole radius $r=105$ nm is the underlying periodic structure. The cavity consists of an air hole, with diameter of 635 nm, which replaces the central hole and its six neighbors. The sample is fabricated on a silicon-on-insulator wafer from SOITEC by means of electron-beam lithography followed by reactive-ion etching, using a three-layer process for transfer of the photonic crystal pattern [10,11]. The silicon oxide layer is then removed by wet etching to obtain a self-standing membrane.

A scanning electron microscope (SEM) image of the sample is provided in the inset of Fig. 1(a). The design and the preliminary theoretical characterization of the cavity modes were performed by means of a guided-mode expansion (GME) method [12]. The main resonant frequency of the cavity is predicted to be near 1300 nm in order to match its resonant frequency with the emission spectrum of PbS quantum dots (QDs) suspended in toluene. A local infiltration apparatus, developed by us for transferring subfemtoliter amounts of liquids inside pores of solid materials [13], permits us to perform a controlled liquid deposition inside the central pore of the cavity. The system makes use of controlled microinfiltration monitored by near-field and confocal microscopy. The thus obtained infiltration can also be canceled again by washing the sample with ethanol and letting it dry inside an oven. This makes the infiltrated photonic pattern rewritable.

The cavity structure with a large central hole is especially suited for local infiltration, and the active silicon microcavity with quantum dots on which we report in this paper is a photonic system that was made with this technique. The emission spectrum of the thus obtained system was collected by using a SNOM with an etched uncoated near-field fiber probe [14] in illumination-collection configuration by exciting the source at 780 nm with an excitation density of roughly 1 MW/cm^2. Near-field microscopy offers an advantageous tool to locally characterize the performances of photonic crystal devices [15–21], and it is necessary to observe the subwavelength spatial distributions of the spectral features associated with the cavity mode that are not accessible with far-field techniques. Figure 1(a) provides a schematic view of the setup. By scanning the sample with the SNOM

*vignolini@lens.unifi.it

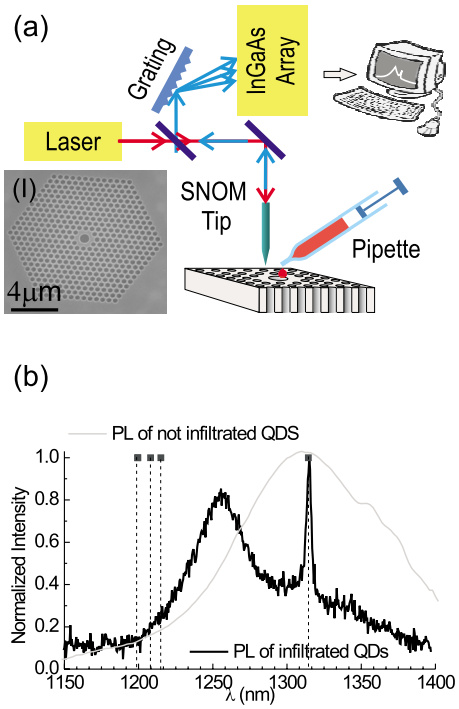

FIG. 1. (Color online) (a) Schematic view of the setup. Laser light is coupled into the SNOM tip and excites the sample. The photoluminescence of the infiltrated QDs is collected through the same tip, dispersed in a monochromator, and detected with a cooled InGaAs diode array. Inset (I): SEM image of the photonic crystal microcavity. (b) Typical photoluminescence spectrum of QDs infiltrated inside the structures (black line) compared with the spectrum of the same QDs outside the cavity (gray line). The dotted lines represent the positions of the calculated modes using the guided-mode expansion method of the structure without including the presence of the QD solution inside the central hole. The calculated main mode of the cavity at 1315 nm is observed in the experimental spectrum, while the modes around 1200 nm are not observed since they do not couple with the near-field probe in the specific point of the sample where the spectrum is taken.

we collect, for each position of the tip, the emission spectrum of the infiltrated QDs. Figure 1(b) shows a typical emission spectrum of the QDs as infiltrated in the microcavity, compared with a reference spectrum of the same QDs in solution. The presence of the cavity induces one defined peak centered at 1315 nm with a full width at half maximum of about 2 nm and a broader band at 1257 nm, showing a frequency redistribution of the photoluminescence signal. The presence of these peaks assures that we are able to couple the emission of the QDs with the photonic crystal cavity modes. As will be shown below, the peak at 1315 nm corresponds to the main (high quality factor) resonant mode.

To map local density-of-states (LDOS) effects, we record photoluminescence spectra at several positions inside (A,B,B') and outside (O) the cavity region. The labeled circles in the topographic image presented in the inset of Fig. 2 indicate the positions where the spectra are collected. By comparing the relative amplitudes between the two peaks at 1257 and 1315 nm it is clear that the emission is strongly

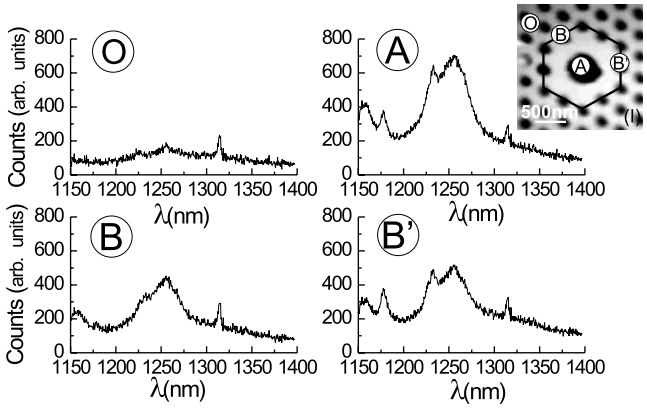

FIG. 2. Near-field spectra collected for different positions as indicated in the shear force topographic image (2×2 μm^2) reported in (I).

dependent on position. In particular, in A the contribution of the broader mode dominates, while outside the cavity region, the mode at 1315 nm is more intense, proving that the two modes have a distinct spatial distribution. The spectra collected in the two symmetric, and therefore ideally indistinguishable, positions (B,B') highlight the role of the disorder in the sample, which can be retraced both to fabrication and to a slightly asymmetric infiltration. Although the integrated signal and the relative amplitudes between the two main cavity modes are quite similar, different peaks, especially at high energy, appear more evident in B' with respect to B. The peak at 1175 nm most probably corresponds to the convolution of the three modes that fall around 1200 nm in the GME calculation. See Fig. 1(b). The broadening and wavelength shift are attributed again to nonideal parameters and disorder in the sample.

The quality factor (Q factor) of the infiltrated microcavity strongly depends on the quality (grade) of the infiltration. The introduction of, e.g., clustered QDs inside the pore, or overfilling of the pore (and spilling of material around it), can decrease the final Q factor. In Fig. 3 typical emission spectra are reported as observed for two different infiltrations. The difference in the quality of the infiltration is clearly visible comparing the topography images. In particular, in the topography image reported in the inset (I), the presence of clustered quantum dots does not permit one to recognize the position of the central hole, while in the case of the inset (II) the central hole is clearly visible in the topographic image.

From the collected data it is possible to reconstruct, for a selected wavelength, the spatial distribution of the emission of the local source. Figures 4(a) and 4(b) show the spatial intensity distribution associated with the cavity peak at a wavelength of 1315 nm and with the broader band at 1257 nm, respectively. The comparison between the experimental images indicates that they present two completely different spatial distributions: while the spatial distribution of the broader band at 1257 nm is concentrated in the center of the cavity, for the other one the maximum of the signal is located outside the cavity region and it presents a preferential axis.

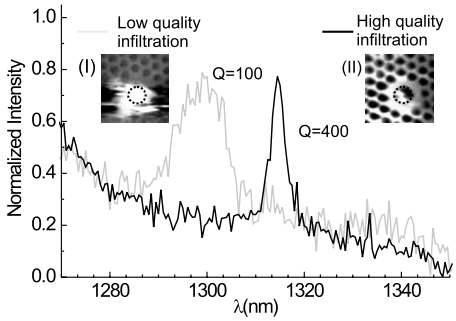

FIG. 3. Near-field spectra related to two infiltrations performed on different samples with the same nominal parameters. If a not perfect infiltration is performed, we obtain a reduction of the Q factor by a factor of 4. In the insets the topography images of the samples for the two different infiltrations are reported; in particular inset (I) presents the topography image (2×2 μm^2) of the sample surface obtained in correspondence with the spectrum in gray line, while inset (II) corresponds to the spectrum in black line.

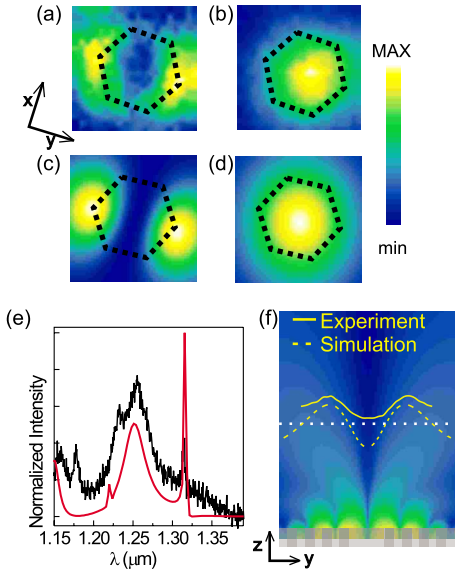

FIG. 4. (Color online) (a),(b) Measured spatial intensity distribution associated to the cavity peak at 1315 nm and to the broader peak at 1257 nm, respectively. (c),(d) Calculated intensity distributions of the electric field component along the x axis [size of images (a) and (d) 2×2 μm^2]. (e), The experimental spectrum obtained integrating all over the image (black line) is compared with the calculated spectrum of the intensity associated with the electric field component along the x axis (red line) over the same scanning region at distance $d=1.36$ μm. (f) Distribution of the intensity of the electric field component along the x axis collected in a vertical plane along the y direction and centered in the middle of the cavity (image size 2.3×3 μm^2). The white dotted line represents the effective height in which the simulated profile of the electric field (yellow dotted line) is collected. The yellow solid lines represent the normalized experimental profile of the cavity mode.

In order to better understand the experimental results we performed a 3D finite difference time domain (FDTD) calculation using a commercial FDTD Maxwell equation solver. We model the system as a free-standing photonic crystal using the nominal parameter of the sample. To optimize the simulation we vary the diameter of the central hole and the refractive index of the Si in agreement with the grid size used in the calculation. To excite the cavity modes, the sources are placed in the central hole, whose refractive index is chosen to be 1.45 as in the experimental configuration. Figures 4(c) and 4(d) show the square of the electric field along the x axis $(E_x)^2$ at a distance $d=1.37$ μm, far from the sample surface, while in Fig 4(e) the experimental spectrum obtained integrating the signal in the whole scanning region is compared with the calculated one.

The exact calculation of what the near-field probe really collects requires, in principle, knowledge of the transfer function of the SNOM tip, which depends on the tip itself. This analysis is practically not feasible, so the problem has to be simplified. To that end, one can assume that the near-field map detected by the tip can be retraced by calculating the theoretical map at an effective distance d from the sample surface [22]. In this way, the value of d does not represent the real height of the tip, but it is an effective free parameter that deals with the fact that the SNOM tip does not collect only the evanescent field of the cavity, but it is also sensitive to the radiative field. Therefore we study how the spatial distribution $(E_x)^2$ varies as a function of the distance d. The case of the mode at 1315 nm is reported in Fig. 4(f). This mode tends to propagate in two separated angular patterns, and the spatial separation between the two lobes increases with d. We find good agreement with the experimental data for $d=1.37$ μm [white dotted line in Fig. 4(f)]. At this distance, the calculated intensity distribution associated with the cavity modes and the spectrum of $(E_x)^2$ reproduces well the experimental results also for the broader peak at 1257 nm as is evident in Figs. 4(c) and 4(d). Moreover, the presence of a preferential symmetry axis observed experimentally can be retraced to the presence of an asymmetry in the central cavity hole, which is also visible in the topographic image provided in the inset (I) of Fig. 2. In particular, we verify in the calculation that when the central hole is elongated along the y direction, with an ellipticity of a few percent, the electric field component along the x axis (E_x) dominates, allowing us to compare our experimental data with the $(E_x)^2$ component calculated in a circular cavity. Altogether, the agreement between theory and experiment is fully satisfactory, demonstrating that the cavity structure is close to design and that the effect of spatial and spectral redistribution on QD emission is due indeed to the occurrence of local cavity modes.

In conclusion, we demonstrate the introduction of a local source in a Si-based photonic crystal microcavity showing the redistribution of the spontaneous emission and the mode profile in this system. The cavity Q and the overall performance of the photonic microstructure in controlling spontaneous emission can be further improved, with the possibility of observing quantum electrodynamical phenomena like the Purcell effect [23] in a silicon environment. Our specific results are potentially useful for applications in the field of integrated emitting structures because they offer, at the same time, the flexibility to exploit local emitters in silicon

substrates and the opportunity to erase and rewrite them. Also, the high sensitivity of the cavity resonance line to local refractive-index variations could be further developed and exploited for nanoscale detection purposes in a silicon environment.

We wish to thank Alfredo de Rossi and the entire micro- and nanophotonics group at LENS for fruitful discussions. This work was financially supported by the European Network of Excellence on nanophotonics Phoremost (Grant No. IST-2-511616-NoE) and by the CARIPLO Foundation.

[1] M. Fujita, S. Takahashi, Y. Tanaka, T. Asano, and S. Noda, Science **308**, 1296 (2005).

[2] D. Englund, D. Fattal, E. Waks, G. Solomon, B. Zhang, T. M. Nakaoka, Y. Arakawa, Y. Yamamoto, and J. Vuckovic, Phys. Rev. Lett. **95**, 013904 (2005).

[3] S. Noda, M. Fujita, and T. Asano, Nat. Photonics **1**, 449 (2007).

[4] S. Strauf, K. Hennessy, M. T. Rakher, Y. S. Choi, A. Badolato, L. C. Andreani, E. L. Hu, P. M. Petroff, and D. Bouwmeester, Phys. Rev. Lett. **96**, 127404 (2006).

[5] K. Hennessy, A. Badolato, M. Winger, D. Gerace, M. Atatüre, S. Gulde, S. Falt, E. L. Hu, and A. Imamoglu, Nature (London) **445**, 896 (2007).

[6] I. Fushman, D. Englund, and J. Vuckovic, Appl. Phys. Lett. **87**, 241102 (2005).

[7] R. Bose, X. Yang, R. Chatterjee, J. Gao, and C. W. Wong, Appl. Phys. Lett. **90**, 111117 (2007).

[8] Z. Wu, Z. Mi, P. Bhattacharya, T. Zhu, and J. Xu, Appl. Phys. Lett. **90**, 171105 (2007).

[9] L. Martiradonna, L. Carbone, A. Tsndaechanurat, M. Kitamura, S. Iwamoto, L. Manna, M. De Vittorio, R. Cingolani, and Y. Arakawa, Nano Lett. **8**, 260 (2008).

[10] M. Belotti, M. Galli, D. Bajoni, L. C. Andreani, G. Guizzetti, D. Decanini, and Y. Chen, Microelectron. Eng. **73**, 405 (2004).

[11] D. Peyrade, Y. Chen, A. Talneau, M. Patrini, M. Galli, F. Marabelli, M. Agio, L. C. Andreani, E. Silberstein, and P. Lalanne, Microelectron. Eng. **61**, 529 (2002).

[12] L. C. Andreani and D. Gerace, Phys. Rev. B **73**, 235114 (2006).

[13] F. Intonti, S. Vignolini, V. Turck, M. Colocci, P. Bettotti, L. Pavesi, S. L. Schweizer, R. Wehrspohn, and D. S. Wiersma, Appl. Phys. Lett. **89**, 211117 (2006); Italian Patent No. TO2006A000216 (2006), Extension Europe, USA 27/09/2007, No. WO2007/107959 A1 (2007).

[14] R. Stöckle, C. Fokas, V. Deckert, R. Zenobi, B. Sick, B. Hecht, and U. P. Wild, Appl. Phys. Lett. **75**, 160 (1999).

[15] P. Kramper, M. Kafesaki, C. M. Soukoulis, A. Birner, F. Muller, U. Gösele, R. B. Wehrspohn, J. Mlynek, and V. Sandoghdar, Opt. Lett. **29**, 174 (2004).

[16] S. I. Bozhevolnyi, V. S. Volkov, J. Arentoft, A. Boltasseva, T. Sondergaard, and M. Kristensen, Opt. Commun. **212**, 51 (2002).

[17] N. Louvion, D. Gerard, J. Mouette, F. de Fornel, C. Seassal, X. Letartre, A. Rahmani, and S. Callard, Phys. Rev. Lett. **94**, 113907 (2005).

[18] A. F. Koenderink, R. Wüest, B. C. Buchler, S. Richter, P. Strasser, M. Kafesaki, A. Rogache, R. B. Wehrspohn, C. M. Soukoulis, D. Ernig, F. Robin, H. Jäckel, and V. Sandoghdar, Photonics Nanostruct. Fundam. Appl. **3**, 63 (2005).

[19] H. Gersen, T. J. Karle, R. J. P. Engelen, W. Bogaerts, J. P. Korterik, N. F. van Hulst, T. F. Krauss, and L. Kuipers, Phys. Rev. Lett. **94**, 073903 (2005).

[20] F. Intonti, S. Vignolini, F. Riboli, A. Vinattieri, D. S. Wiersma, M. Colocci, L. Balet, C. Monat, C. Zinoni, L. H. Li, R. Houdre, M. Francardi, A. Gerardino, A. Fiore, and M. Gurioli, Phys. Rev. B **78**, 041401(R) (2008).

[21] F. Intonti, S. Vignolini, F. Riboli, A. Vinattieri, D. S. Wiersma, M. Colocci, M. Gurioli, L. Balet, C. Monat, L. H. Li, N. Le Thomas, R. Houdré, A. Fiore, M. Francardi, A. Gerardino, F. Roemer, and B. Witzigmann, Physica E (Amsterdam) **40**, 1965 (2008).

[22] Y. De Wilde, F. Formanek, R. Carminati, B. Gralak, P. Lemoine, K. Joulain, J. Mulet, Y. Chen, and J. Greffet, Nature (London) **444**, 740 (2006).

[23] E. M. Purcell, Phys. Rev. **69**, 674 (1946), see p. 681.